

OBJECT-ORIENTED MEASUREMENT OF PIPE SYSTEMS USING EDGE MATCHING AND CSG MODELS WITH CONSTRAINTS

Johan W.H. Tangelder, George Vosselman, Frank A. van den Heuvel
Delft University of Technology, The Netherlands
Faculty of Civil Engineering and Geosciences, Department of Geodesy
{j.w.h.tangelder,g.vosselman,f.a.vandenheuvel}@geo.tudelft.nl

Working Group V/2

KEY WORDS: CAD, error propagation, object-oriented, photogrammetry, reconstruction

ABSTRACT

A method for the measurement of pipe systems from a collection of images is presented. A predefined library of parameterized object models defined by CSG trees is used to describe several types of piping elements. An initial measurement of each component of the pipe system is obtained by selecting the appropriate model from the library, projecting this model into the images and modifying the pose, and the shape of the model such that it is aligned with the object in the images. The images are taken with a calibrated camera. In addition, the exterior orientations of the images are assumed to be known approximately. All the selected models are combined in one tree, that describes the complete pipe system. Constraints within object models and also between object models are applied.

For the precise measurement of pipe systems we developed a two stage fitting procedure. First, in a pixel based fitting stage the model edges are optimally aligned with the pixels with high gradients in a buffer around the projected model edges. Second, in an edge-model based fitting stage the grey values in the buffer are matched with the grey values predicted by a Gaussian smoothed step edge and the standard deviations of the measured parameter values are estimated. The practical application of this fitting procedure is demonstrated using object models with constraints. The use of constraints reduced the standard deviation of most of the estimated parameter values significantly.

1 INTRODUCTION

Piping installations are usually built with a limited number of standardized components, like e.g. straight pipes, curved pipes, connecting elements and more complex elements like valves and tanks. Constructive Solid Geometry (CSG) is an appropriate representation scheme to model piping installations (Ermes and van den Heuvel, 1998). A CSG model is a tree-like structure in which primitive shapes are combined using volumetric Boolean operations (union, intersection, difference) to form more complex shapes. A typical set of primitives contains shapes such as a box, a sphere, a cylinder, a torus, a prism, etc. Each primitive can be parameterized by its position, orientation, and shape (e.g. length and radius for a cylinder). With a CSG tree these primitive elements are combined to represent more complex, composite objects like flanged pipes and T-junctions. Finally, the piping installation itself can be described by one CSG tree that combines the CSG trees of its primitive elements.

In (Tangelder et al., 1999) we presented a pixel based fitting method using CSG primitives for the measurement of objects in images. In this paper that method is extended to object models consisting of CSG trees with constraints as well as to sets of object models sharing constraints. Further, to the fitting procedure an edge-model based fitting stage is added, that estimates the standard deviations of the measured parameters. The companion paper (Ermes, 2000) focuses on the mathematical formulation of the different constraints within and between CSG models. The fitting procedure is discussed in this paper.

Piping installations are generally very complex and images of these installations can show many piping elements. Measurement problems may arise when piping elements are occluded by other elements or when reflections and shadows are disturbing the boundaries of the piping elements. These characteristics of the piping application do not allow a high degree of automation of the measurement process. Therefore, based on photogrammetry and CAD we have implemented a semi-automatic procedure to measure the pose and the shape of a piping element from a collection of images. The images are taken with a calibrated camera. In addition, the exterior orientations of the images are assumed to be known approximately. The measurement procedure consists of the following two steps.

1. Selection of an appropriate object model from the library by the image analyst. In each image a projection of the wire frame of this object model is displayed. The image analyst aligns the edges of these projections with the boundaries of the object in the images. For this purpose the image analyst selects a number of points on the edges in the images and drags these points to the object boundary. For each measured point a linearized observation equation is set up with a user defined weight (Ermes et al., 1999). Also, the exterior orientations of the images are estimated precisely by a bundle adjustment procedure using the obtained object models.
2. Computation of the pose and the shape of the object by fitting the edges of the object model to the boundary pixels in the images. The fitting procedure consists of a **pixel based fitting** stage and an **edge-model based fitting** stage. In the pixel based fitting stage the pose and the shape of the object is computed by fitting the edges of the object model to pixels with high grey value gradients using an iterative least-squares estimation. For each pixel in a buffer around the projected model edges a linearized observation equation is set up weighted by the squared grey value gradient at the pixel (Tangelder et al., 1999). In the edge-model based fitting stage the grey values in the buffer are matched with the grey values predicted by a Gaussian smoothed step edge and the standard deviations of the measured parameter values are estimated. Again for each pixel in the buffer a linearized observation equation is set up as described later in this paper.

To reduce the complexity of the measurement process the image analyst measures piping elements like straight pipes, flanged pipes, T-junctions, flanged curved pipes, etc. one by one. After the first piping element is measured, the image analyst selects a neighboring piping element next. Then, the selected piping element is measured taking into account its internal constraints and the external constraints with its neighbors. The measurements by the image analysts, the constraints, and the fitting measurements are all formulated as weighted observation equations.

The organization of the paper is as follows. In the next section related work is discussed. In section 3 the fitting procedure is outlined. In section 4 we focus on the implementation of the fitting procedure. Practical results are presented in section 5. We conclude in section 6.

2 RELATED WORK

In order to reconstruct a 3D model from a collection of 2D images of an object, (Rockwood and Winget, 1997) define an energy function between the object's images and corresponding images of an articulated mesh representing the 3D object. Then the 3D model is reconstructed by repeated adjustment of the mesh using simulated annealing to minimize the energy function. (Fua, 1996) uses an energy function to fit a polyhedral object model to a collection of 2D images of an object. The energy function is defined as the negative sum of the absolute grey value gradients along the edges of the object in the images. With a steepest gradient method the positions of the corners of the polyhedral model are adapted such that the value of the energy function is minimized. (Lowe, 1991) describes a least-squares algorithm that fits the projected edges to edge pixels. These edge pixels are defined as the pixels with a grey value gradient above some preset threshold. The errors in the approximate alignment of the object model are quantified by the perpendicular distances of the edge pixels to the nearest edge. The fitting algorithm estimates the changes to the values of the pose and shape parameters, that minimize the square sum of these distances. (Sester and Förstner, 1989) describe a clustering algorithm followed by a robust estimation of pose and shape parameters. Their approach is based on correspondences between the edges projected in the images and straight edges that are extracted from the image. (Vosselman and Veldhuis, 1999) compared the performance of Fua's and Lowe's approach and found that the latter approach is much faster due to the comparatively large number of iterations required by the former method. Therefore, we selected also a least-squares approach for our object reconstruction method. (Debevec et al., 1996) describe a system for modeling and rendering architecture from photographs. The image analyst instantiates parameterized geometric primitives such as boxes, prisms, and surfaces of revolution. Measurements are done by marking edges in the images and corresponding edges in the images to the model. Compared to Debevec's approach our approach includes curved object models like curved pipes. (Löcherbach, 1994) describes a fitting approach to reconstruct agricultural land-use areas from remotely sensed images. Based upon a smoothed edge model the boundaries of the land-use units are reconstructed by an iterative least-squares approach.

3 FITTING

After the shape and the pose of an object have been approximated by the measurements of the image analyst, the fitting procedure is invoked to measure the object precisely as well as to estimate the standard deviation of the measured parameter values. Both for the pixel based fitting stage and the edge-model based fitting stage observation equations are set up as described below. Since these observation equations are nonlinear the observation equations are solved using an iterative weighted least-squares approach.

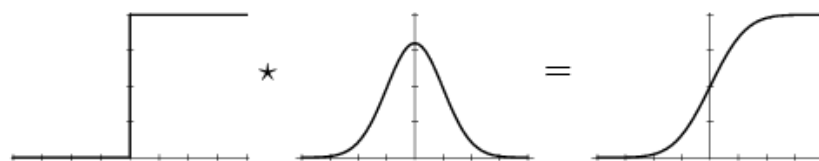


Figure 1: The transition $h(x)$ in (2) between an object and the background (right) is modeled by a step edge (left) smoothed with a Gaussian (middle).

3.1 Pixel Based Fitting

A direct relationship between the estimation of the pose and shape parameters and the gradients of the pixels can be achieved by modifying the approach by (Lowe, 1991). Lowe introduces an observation equation for each pixel which fulfills two conditions: (1) the grey value gradient should be above some threshold and (2) the pixel should be within some range of a projected edge. We follow (Vosselman and Veldhuis, 1999) in dropping the first condition: i.e., for all pixels within some range of a projected edge, the observation equation is introduced. In order to ensure that the pixels with the higher gradients dominate the parameter estimation, the squared grey value gradients of the pixels are used as weights to the observation equations: i.e.,

$$\Delta u_j = \sum_{i=1}^n \left(\frac{\partial u}{\partial p_i} \right)_j \Delta p_i, \quad W\{\Delta u_j\} = \left(\left(\frac{\partial g}{\partial u} \right)_j \right)^2, \quad (1)$$

where Δu_j ($1 \leq j \leq m$) is the signed distance from the j^{th} pixel to the projected model edge and $(\partial g / \partial u)_j$ is the grey value gradient at the pixel perpendicular to the model edge.

Note, that in the pixel based approach Δu_j is not stochastic. Therefore, it is not possible to estimate the standard deviations of the obtained parameter values by propagation of the standard deviation of the observations. In the edge-model based fitting approach presented next, the standard deviation of the observations is propagated to the parameter values. Practical experience showed that the edge-model based approach requires better approximate positioning by the image analyst than the pixel based approach. Therefore, we decided not to replace the pixel based approach but to apply both. In our implementation first the model edges are shifted to the object boundaries in the images by pixel based fitting. Then by edge-model based fitting the model edges are shifted to their final position according to the Gaussian smoothed step edge model described below. Also, the standard deviations of the obtained parameter values are estimated.

3.2 Edge-Model Based Fitting

The edge-model based fitting approach compares the grey values predicted by the Gaussian smoothed step edge with the grey values in the actual image. We apply the principle of differential matching described by (Förstner, 1993) to estimate a shift of the model edges and to propagate the standard deviation in the grey values to the standard deviation of the obtained parameter values.

The edge-model based fitting procedure matches the grey values in a buffer around the projected edges of an object model with the grey values predicted by a Gaussian smoothed step edge. A Gaussian smoothed step edge predicts the grey value at a pixel depending on its signed distance x to the transition between the object and the background. We denote the Gaussian smoothed step edge by the function h and the grey values by the function g .

At the transition between the object and the background there is a discontinuous change of the grey value, that can be described by a step function. Due to the image formation process this transition loses its sharpness in the images. This is modeled by smoothing the step edge with a Gaussian as illustrated by Fig. 1. The obtained Gaussian step edge h predicts the grey values at the pixel by

$$h(x) = h_{start} + (h_{end} - h_{start}) I(x), \quad (2)$$

where x is the signed distance of the pixel to the transition between the object and the background. h_{end} and h_{start} denote the grey values of the object and the background. The Gaussian integral I is defined by

$$I(x) = \frac{1}{\sigma_s \sqrt{2\pi}} \int_{-\infty}^x e^{-t^2 / (2\sigma_s^2)} dt \quad (3)$$

As $I(x)$ ranges from 0 to 1, $h(x)$ ranges from h_{start} to h_{end} . The parameter controlling the amount of smoothing is σ_s .

For each pixel within some range of the projected model edges an observation equation is set up as follows.

First, the shift Δx_j between the projected model edge and the transition between the object and the background is related to the difference of the observed grey value and the predicted grey value at the pixels divided by the first derivative of the smoothed step edge, i.e.

$$\Delta x_j = (h(x_j) - g(x_j)) / h'(x_j), \quad (4)$$

where x_j ($1 \leq j \leq m$) is the signed distance at the j^{th} pixel to the projected model edge and $g(x_j)$ is the grey value at the pixel.

The linearized equation

$$\Delta x_j = \sum_{i=1}^n \left(\frac{\partial x}{\partial p_i} \right)_j \Delta p_i, \quad (5)$$

relates this shift Δx_j to the adjustments to the parameter values Δp_i . In this equation $(\partial x / \partial p_i)_j$ is the partial derivative of the signed distance at the j^{th} pixel to the projected edge with respect to the parameter p_i . (Ermes et al., 1999) describes an analytical approach to compute these partial derivatives efficiently. By combining the last two equations we obtain the observation equation

$$E\{\Delta g_j\} = E\{h(x_j) - g(x_j)\} = \sum_{i=1}^n \left(\frac{\partial x}{\partial p_i} \right)_j h'(x_j) \Delta p_i, \quad (6)$$

that directly relates the difference of the actual and predicted grey value at a pixel with the adaptations of the parameter values. After each iteration step the standard deviation σ_g of Δg_j is estimated from the residuals of the least-squares fit by

$$\hat{\sigma}_g = \sqrt{\frac{\sum_{j=1}^m (h(x_j) - g(x_j))^2}{m - n}} \quad (7)$$

For each pixel within some range of the projected model edges an observation equation (6) is set up with weight $1/\hat{\sigma}_g^2$, where $\hat{\sigma}_g$ is computed at the previous iteration step. Further, the constraints are included in the adjustment as weighted linearized observation equations (Ermes, 2000). All the parameters (pose and shape) are directly related to primitives in the CSG tree.

The parameter values are adjusted with the weighted least-squares estimates of Δp_i . The projections of the model edges are updated and the weighted least-squares adjustment described above is repeated until the adjustment of each parameter value divided by its estimated standard deviation is smaller than a predefined error bound or the relative improvement of the estimated standard variation $\hat{\sigma}_g$ is below a predefined threshold.

4 IMPLEMENTATION ASPECTS

The software is developed in C++ on a Silicon Graphics Workstation using the ACIS kernel. ACIS is an object-oriented software library with CAD functionality, such as CSG object modeling and hidden-line analysis. For the visualization of the images and the CAD models OpenGL is used. OpenGL is a software interface for the graphics hardware on a computer. It allows the fast and interactive viewing of the image data and the CAD models.

After an object model is aligned approximately to an object in the images by the image analyst, it is measured precisely by the fitting procedure. First the iterative pixel based fitting stage is started. A grid, that consists of a number of profiles perpendicular to a projected model edge, is defined in this buffer. After each iteration the profile length is halved. The profiles are shrunk until each profile contains three points at a distance of one pixel as shown in Fig. 2. (Tangelder et al., 1999) provides a more detailed description of the implementation of the pixel based fitting stage. Then the final iteration of the pixel based fitting stage is executed. Next, the iterative edge-model based fitting stage is started. An iteration consists of the following steps:

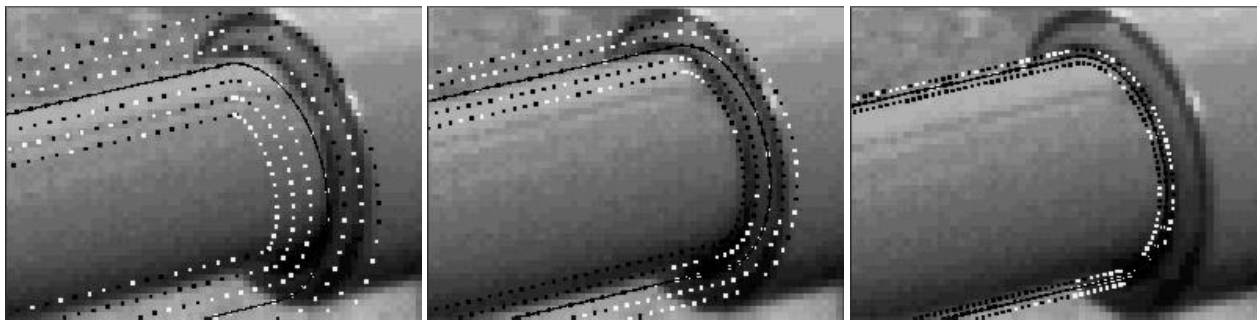


Figure 2: The fitting algorithm shrinks the buffer around the projected edges of the cylindrical model while keeping the number of grid points equal. Only if the direction of the grey value gradient is approximately perpendicular to the nearest projected edge of the cylinder (black grid point) an observation equation is set up. The grid points, at which no observation equation is set up, are white. This has the advantage that non-perpendicular gradients caused by background objects will not interfere the fitting procedure.

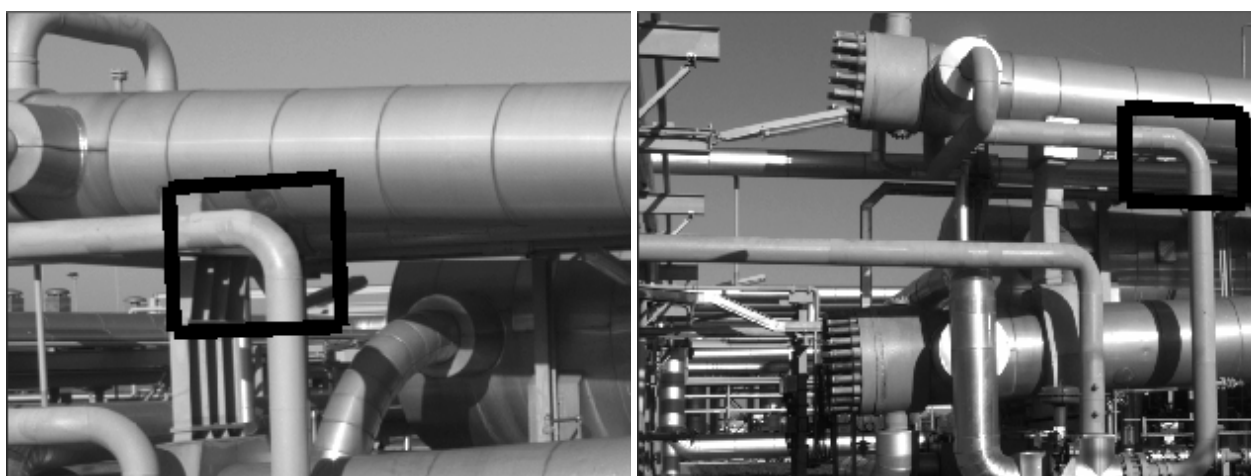


Figure 3: Digital images of an installation at a production cluster of the Groningen gas field.

1. Given the approximate pose and shape parameters of the object and the pose parameters for each image, the wire frames of the visible model edges are projected in the images. ACIS computes these visible model edges by a hidden line analysis based on the perspective projection.
2. Observation equations are set up for the pixels in a buffer around the projected model edges. All profiles have a length of 2.0 pixels. On the profile the signed distance to the projected model edge ranges from -1.0 pixel to 1.0 pixel. With each profile a smoothed step edge is associated based upon equation (2). In this smoothed step edge function σ_s has a predefined constant value (currently set to 1.0). In the first iteration the values h_{start} and h_{end} are set to the grey values at signed distance -2.0 and 2.0 pixel, respectively. In the remainder of the procedure for each profile its step edge model is fixed, i.e. the values of h_{start} and h_{end} are not changed. For the signed distance $x = -1.0$, $x = 0.0$ and $x = 1.0$ pixel observation equations are set up as described in the previous section.
3. Finally, the observation equations are solved and convergence of the iteration process is tested as described in the previous section.

5 PRACTICAL RESULTS

For the evaluation of the developed measurement method a pilot project was carried at a production cluster of the Groningen gas field, which is exploited by the Nederlandse Aardolie Maatschappij (NAM). A dataset consisting of 100 photographs of this cluster has been obtained in half a day using a digital camera (Kodak DCS 420). Each image comprises 1524x1012 pixels. A length of 1 pixel corresponds with 2 to 20 mm in reality. Fig. 3 shows an installation that is part of this cluster. In this section we focus on the measurement of the curved pipe connected to the horizontal and vertical straight pipe enclosed by the rectangle in Fig. 3. Using four images, we measured these pipes with the fitting procedure. Also, we investigated the effect of the use of constraints on the pipe models on the standard deviations of the obtained parameter values. In the remainder of this paper we express coordinates, lengths and radii in millimeters and angles

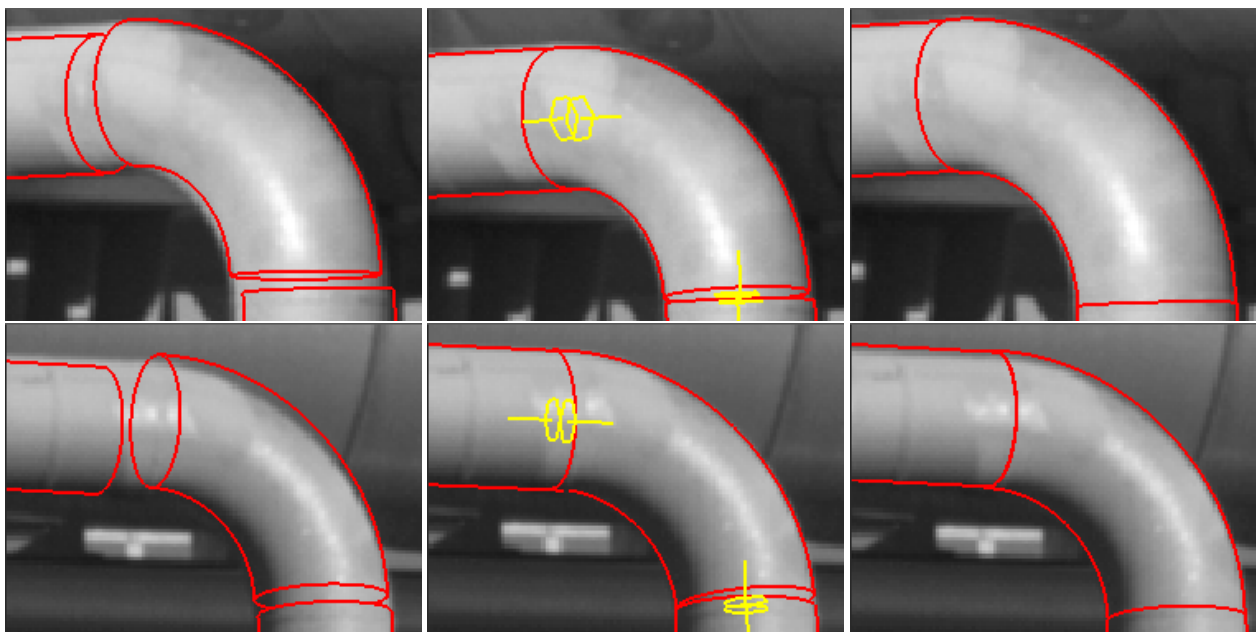


Figure 4: Measurement of pipes. The left two images show the pose and the shape of the pipes before the fitting procedure starts. The middle two images show the result using no constraints and the right two images show the result using constraints.

in degrees. We measured the two straight pipes and the curved pipe with the parameterized cylinder and torus models described below.

A straight piping element is modeled by a cylinder that is rotation symmetric around its axis. Hence, the orientation of the cylinder is defined by the direction of its axis. This direction is specified by a normalized vector (t_0, t_1, t_2) relatively to a reference coordinate system. Hence, the pose and the shape of the cylinder is described singularity-free by three parameters x, y and z denoting its position, three parameters t_0, t_1 and t_2 denoting its orientation, and two shape parameters l and r denoting its length and radius, respectively.

A curved piping element is not symmetric around an axis and therefore its orientation is defined by a normalized quaternion vector (q_0, q_1, q_2, q_3) providing a singularity-free representation of rotation (Ermes et al., 1999). A curved piping element has the shape of a torus. The center line of the pipe is a circle with a major radius R . A torus is obtained by sweeping the center of a smaller circle with a minor radius $r < R$ along the center line of the piping element. The boundary of the torus is the surface swept out by the circle. An angle denotes the part of the center line of the piping element that is followed. For instance a curved pipe between two perpendicular straight pipes is described by a torus with an angle of 90 degrees. Therefore, we model this piping element by a torus described by three parameters x, y and z denoting its position, four normalized quaternion parameters q_0, q_1, q_2 and q_3 denoting its orientation, and two shape parameters r and R denoting its minor and major radii, and a shape parameter ω denoting the torus angle.

One end of the curved pipe is connected to the horizontal straight pipe and the other end is connected to the vertical straight pipe. Therefore, for each curved pipe end the image analyst has to add a position constraint and a direction constraint both with a high weight. These constraints ensure that the curve pipe ends meet with the straight pipe ends and have identical orientations.

Fig. 4 shows the three pipes after the measurements by the image analyst, after fitting without constraints and fitting with constraints. In the test the predefined error bound and the predefined threshold described at the end of section 4 have been set to 0.01 and 0.001, respectively. In the test the fitting procedure takes about 30 seconds CPU time.

Table 1 compares fitting with and without constraints. The differences between the obtained parameter values, and the standard deviations in both cases are shown. The standard deviations above 0.5 are printed bold. Also, the adjustment of the parameter values by the edge-model based fitting stage is shown. For fitting without constraints a lot of parameters are difficult to estimate, because the transitions at the pipe ends are smooth. Therefore, in the case of fitting using no constraints the differences between the positions of the pipe ends are rather high: $(-6.15, 3.86, -12.32)$ for the horizontal and the curved pipe and $(-0.95, -34.58, 0.85)$ for the vertical and the curved pipe. Since the pipes are physically connected, these positions should be identical. Therefore, using a high weight on the position constraints described above is justified. The difference between the normalized direction vectors for the horizontal and the end of the curved pipe is

	difference by using constr.	σ_p using no constr.	σ_p using constr.	difference by edge-model based fitting
H				
x	22.66	1.35	0.24	0.14
y	-29.63	2.62	0.93	-0.87
z	4.04	0.29	0.22	1.89
t_0	$38.4 \cdot 10^{-3}$	$1.2 \cdot 10^{-3}$	$0.3 \cdot 10^{-3}$	$-5.8 \cdot 10^{-3}$
t_1	$-0.7 \cdot 10^{-3}$	$0.01 \cdot 10^{-3}$	$0.007 \cdot 10^{-3}$	$0.2 \cdot 10^{-3}$
t_2	$-2.7 \cdot 10^{-3}$	$0.2 \cdot 10^{-3}$	$0.2 \cdot 10^{-3}$	$1.4 \cdot 10^{-3}$
l	-18.69	3.10	1.29	-6.11
r	-1.57	0.15	0.16	-1.67
C				
x	-7.5	0.67	0.19	2.01
y	3.94	0.47	0.16	-0.84
z	-28.32	2.23	0.91	1.59
q_0	$-21.1 \cdot 10^{-3}$	$3.9 \cdot 10^{-3}$	$0.1 \cdot 10^{-3}$	$2.9 \cdot 10^{-3}$
q_1	$20.8 \cdot 10^{-3}$	$3.2 \cdot 10^{-3}$	$0.06 \cdot 10^{-3}$	$0.5 \cdot 10^{-3}$
q_2	$28.6 \cdot 10^{-3}$	$3.4 \cdot 10^{-3}$	$0.05 \cdot 10^{-3}$	$-0.2 \cdot 10^{-3}$
q_3	$0.4 \cdot 10^{-3}$	$0.1 \cdot 10^{-3}$	$0.009 \cdot 10^{-3}$	$0.1 \cdot 10^{-3}$
R	9.74	1.53	0.96	0.47
r	-8.15	0.17	0.22	-0.09
ω	1.56	0.44	0.01	-0.10
V				
x	0.79	0.23	0.22	-0.71
y	0.07	0.18	0.18	0.21
z	0.30	3.27	3.40	1.32
t_0	$-0.7 \cdot 10^{-3}$	$0.1 \cdot 10^{-3}$	$0.1 \cdot 10^{-3}$	$0.9 \cdot 10^{-3}$
t_1	$0.1 \cdot 10^{-3}$	$0.1 \cdot 10^{-3}$	$0.1 \cdot 10^{-3}$	$0.3 \cdot 10^{-3}$
t_2	$0.002 \cdot 10^{-3}$	$0.007 \cdot 10^{-3}$	$0.007 \cdot 10^{-3}$	$0.005 \cdot 10^{-3}$
l	-14.1	4.20	3.52	0.25
r	0.22	0.08	0.07	0.05

Table 1: Comparison of fitting with and without constraints for the curved (C) pipe connected to the horizontal (H) and vertical (V) straight pipe. The first column shows the differences of the obtained parameter values for fitting with and without constraints. The second and third column compare the standard deviation (σ_p) for using no constraints and using constraints. The fourth column shows the difference of the parameter values by the edge-model based fitting stage.

($3.6 \cdot 10^{-3}$, $-0.5 \cdot 10^{-3}$, $32.8 \cdot 10^{-3}$). Between the vertical and the curved pipe it is ($-42.3 \cdot 10^{-3}$, $-57.0 \cdot 10^{-3}$, $-2.3 \cdot 10^{-3}$). Hence, we assume that the physically connected pipes have the same direction and we use a high weight on the direction constraints, also. Checking the trustworthiness of the constraints as described above is rather cumbersome. A tool based on statistical analysis should be developed to assist the image analyst with this task. Applying the constraints reduces the standard deviations of most of the parameter values. For the horizontal pipe only, the position y and the length l still cannot be estimated very well. Since the position of a pipe end depends on y , y is correlated strongly with the length of the pipe l . Similar, for the vertical pipe z and l cannot be estimated very well and are also correlated strongly. For the curved pipe the same is true for z and R . In all these cases this is due to the smooth transitions between the pipes. Compared to the difference in parameter values caused by using constraints the adjustment of the parameter values by the edge-model based fitting stage is small.

6 CONCLUSIONS

In this paper we presented a new approach for precise fitting of parameterized object models to objects in images. A direct relationship between the pose and shape parameters and the grey values at the object boundaries has been formulated using a smoothed step edge model. A fitting procedure using a weighted iterative least-squares method to estimate the parameter values and their standard deviations has been developed and implemented. The practical application of this fitting technique has been demonstrated using object models with constraints. The use of constraints reduced the standard deviation of most of the estimated parameter values significantly.

In the current implementation checking the trustworthiness of the constraints is rather cumbersome. Therefore, further research focuses on the development of a tool based on statistical analysis to assist the image analyst with this task.

ACKNOWLEDGMENTS

We thank the Nederlandse Aardolie Maatschappij (NAM) for supporting the pilot project at a production cluster of the Groningen gas field. This research was supported by the Dutch Technology Foundation (STW).

REFERENCES

- Debevec, P., Taylor, C. and Malik, J., 1996. Modeling and rendering architecture from photographs: A hybrid geometry- and image-based approach. In: H. Rushmeier (ed.), *Proceedings of SIGGRAPH 96*, Addison Wesley, pp. 11–20.
- Ermes, P., 2000. Constraints in CAD models for reverse engineering using photogrammetry. In: *IAPRS*, Vol. 32, part 5B.
- Ermes, P. and van den Heuvel, F., 1998. Measurement of piping installations with digital photogrammetry. In: *IAPRS*, Vol. 32, part 5, pp. 217–220.
- Ermes, P., van den Heuvel, F. and Vosselman, G., 1999. A photogrammetric measurement method using CSG models. In: *IAPRS*, Vol. 32, part 5W11, pp. 36–42.
- Förstner, W., 1993. Image matching. In: R. Haralick and L. Shapiro, *Computer and Robot Vision*, Vol. II, Addison-Wesley, Reading, Massachusetts, chapter 16, pp. 289–378.
- Fua, P., 1996. Model-based optimization: Accurate and consistent site modeling. In: *IAPRS*, Vol. 31, part B3, pp. 222–233.
- Löcherbach, T., 1994. Fusion of multi-sensor images and digital map data for the reconstruction and interpretation of agricultural land-use units. In: *IAPRS*, Vol. 30, part 3, pp. 505–511.
- Lowe, D., 1991. Fitting parameterized three-dimensional models to images. *IEEE Transactions on Pattern Analysis and Machine Intelligence* 13(5), pp. 441–450.
- Rockwood, A. and Winget, J., 1997. Three-dimensional object reconstruction from two-dimensional images. *Computer-Aided Design* 29(4), pp. 279–285.
- Sester, M. and Förstner, W., 1989. Object location based on uncertain models. In: *Mustererkennung 1989*, Informatik Fachberichte 219, Springer Verlag, pp. 457–464.
- Tangelder, J., Ermes, P., Vosselman, G. and van den Heuvel, F., 1999. Measurement of curved objects using gradient based fitting and CSG models. In: *IAPRS*, Vol. 32, part 5W11, pp. 23–30.
- Vosselman, G. and Veldhuis, H., 1999. Mapping by dragging and fitting of wire-frame models. *Photogrammetric Engineering & Remote Sensing* 65(7), pp. 769–776.